RSC Advances

PAPER

View Article Online
View Journal | View Issue

Cite this: *RSC Adv.*, 2025, **15**, 8901

Task-specific deep eutectic solvents with synergistic catalytic performance as excellent and recyclable catalysts for Beckmann rearrangement†

Shiqin Sun, [a] Yanshun Li[a] and Shiwei Liu*[b]

Received 18th February 2025
Accepted 14th March 2025

DOI: 10.1039/d5ra01178g

rsc.li/rsc-advances

Novel "task-specific" deep eutectic solvents (DESs) were synthesized and were used in the Beckmann rearrangement reaction to prepare ε-caprolactam, with DES $[InCl_3][AA]_2$ achieving 100% cyclohexanone oxime (CHO) conversion and 99.5% ε-caprolactam (CPL) selectivity under 80 °C for 2 h. This "task-specific" approach gives some advantages to the reaction, such as rapid reaction speed, high yield of the target product, easy catalyst recovery, and good universality, making the DES catalytic system of great academic significance and have potential application prospects.

1 Introduction

ε-Caprolactam (CPL) is a significant organic chemical raw material utilized in the production of various industrial products, including nylon fibers, nylon-6 engineering plastics, as well as pharmaceuticals, coatings, plasticizers, and artificial leather, *etc.*[1] CPL is industrially produced *via* Beckmann rearrangement, which is a well-known reaction in organic chemistry.[2] However, its production process has some drawbacks such as poor reaction orientation, numerous side reactions, and cumbersome product separation steps, especially the difficulty in separating, recycling, and regenerating catalyst sulfuric acid, as well as serious waste acid emissions.[3] Therefore, the reaction using a catalyst with an excellent catalytic performance and outstanding reusability has become a focus, as well as the difficulty in the preparation of ε-caprolactam.

In order to overcome the problems of sulfuric acid catalyst, researchers have investigated and developed diverse solid catalyst types (Table 1), including oxides,[4,5] metal phosphates,[6] and molecular sieve catalysts,[7,8] and used them to catalytic product CPL in gas–solid two-phase system.[9] Although the aforementioned catalytic system attained high conversion rates and selectivity, the gas-phase Beckmann rearrangement necessitates elevated temperatures (exceeding 300 °C), leading to swift carbon accumulation and coking on the active sites, which results in the rapid deactivation of the catalyst.[10]

The liquid phase rearrangement reaction has been gotten a lot of attentions due to its easy operation, mild reaction conditions, and low energy consumption. As a result, various new catalytic reaction systems, such as inorganic/organic acids,[11,12] solid acids/molecular sieves,[13–15] ionic liquids,[16–18] *etc.*, have been investigated in the liquid-phase rearrangement reactions. However, these catalytic systems also have inevitable drawbacks, such as expensive raw materials, harsh reaction conditions, complex synthesis processes, or poor repeatability. Therefore, it is seen that strengthening the technological innovation of ε-caprolactam production process has important academic significance and potential application prospects.[19]

As a novel form of environmentally friendly catalytic material, deep eutectic solvents (DESs) have the characteristics of easy availability of synthetic raw materials, simple preparation, no-volatilization, good thermal stability, dual function of medium/catalyst, adjustable structure and acidity, easy separation-recovery-reusability, strong universality, *etc.*[20–22] DESs find extensive application in various domains, including extraction separation,[23] electrochemistry,[24] functional materials,[25] and chemical catalysis.[26] Especially, it has been successfully used in many organic reactions and exhibits excellent catalytic performance.[27,28]

In our prior research, a series of Brønsted acidic and Lewis acid DESs were prepared and utilized to catalyze the liquid-

Table 1 Beckmann rearrangement results of various catalysts reported in recent years

Catalysts	T/°C	t/h	C_{CHO}/%	S_{CPL}/%	Y_{CPL}/%	References
B_2O_3/ZrO_2	300	6	97.7	97.0	94.8	4
Ta_2O_5/SiO_2	300	100	96.5	97.5	94.1	5
$AlPO_4$-γAl_2O_3	300	6	—	—	73.1	6
HY	380–390	20	58.0	76.0	44.1	7
MCM-41	350	6	100	92.0	92.0	8

[a]*Department of Biological and Chemical Engineering, Shandong Vocational College of Science and Technology, 6388 West Ring Road, Weifang 261021, People's Republic of China*

[b]*College of Chemical Engineering, Qingdao University of Science and Technology, 53Zhengzhou Road, Qingdao 266042, People's Republic of China. E-mail: liushiweiqust@126.com*

† Electronic supplementary information (ESI) available. See DOI: https://doi.org/10.1039/d5ra01178g

phase Beckman rearrangement reaction. The results demonstrated that these DESs exhibited exceptional catalytic performance, reusability, and versatility.[29–31] Nonetheless, all the DESs studied previously were mono-acidic, possessing limited tunability in terms of acid type and acid strength. This limitation hindered the selection of a more optimal catalyst. To the best of our knowledge, there has been no published literature on the synthesis of bi-acidic DES and its application in catalyzing rearrangement reactions. Subsequently, zinc chloride based DESs were used to catalyze rearrangement reactions and achieved good catalytic effects. The experimental results indicate that the strong chelating ability of zinc active sites is a key factor in the reaction,[32,33] which reduces the activation energy and provides a smooth channel for the reaction. Therefore, we screened out the preparation of the task-specific DESs with Lewis acidic $InCl_3$ having stronger coordination and complexation ability and some Brønsted organic acid, and used for catalytic rearrangement reaction, hoping to achieve better catalytic effects. The DES $[InCl_3][AA]_2$ demonstrated exceptional catalytic performance, even at a temperature of 80 °C for a duration of 2 h. The conversion of cyclohexanone oxime and the selectivity for ε-caprolactam were both remarkable, reaching 100% and 99.5%, respectively. This achievement was credited to the strong complexing capacity of the In active center, along with the synergistic catalytic influence of Brønsted and Lewis acid sites present in the DES. Additionally, the specialized DES $[InCl_3][AA]_2$ showed good reusability and broad applicability in the reaction. If taking the Cr(III)-based DES catalytic system as an example,[31] compare the performance, efficiency, and sustainability metrics (*e.g.*, catalyst reusability, reaction conditions, and environmental impact) with$[InCl_3][AA]_2$ respectively. The results showed that under the same temperature, the reaction time required for the $[InCl_3][AA]_2$ catalytic system was shorter (2 h) and the catalyst dosage was reduced by 20.0% when achieving the same reaction effect. In terms of performance, experimental data shows that $[InCl_3][AA]_2$ exhibits a higher yield (99.5%), which is 0.8% higher than DES based on Cr(III). From the perspective of environmental impact, $[InCl_3]$[AA]-DES does not contain toxic heavy metal Cr(III), reducing potential harm to the environment.

2 Experimental

2.1. Materials

Cyclohexanone oxime (CHO), indium chloride ($InCl_3$), benzoic acid (BA), formic acid (FA), acetic acid (AA), and propionic acid (PA) were purchased from Aladdin Biochemical Technology Co., Ltd. Dichloromethane was obtained from Xilong Chemical Co., Ltd (China). All starting materials, reagents and solvents were used without further purification.

2.2. Synthesis of DESs

The DESs were prepared by a single-step process under inert gas atmosphere (N_2) at atmospheric pressure. The specified quality of HBA ($InCl_3$) and HBD (Brønsted acids: FA, AA, PA or PPA) were mixed and reacted at 60 °C until the transparent homogenous liquids were given (Fig. S1†). The structures of HBA ($InCl_3$) and HBD (Brønsted acids) are shown in Fig. S2.† Some characterizations were used to characterize or test the chemical structure and property of synthesized DES. The FT-IR spectra were performed by a Nicolet IS10. ^{1}H NMR spectra were performed on a Bruker Advance 600. The acid strength of DES was measured by a pH meter. The thermogravimetric analysis (TG) was carried out on a German Netzsch TG-209. DFT calculations were performed using Gaussian software (Gaussian 09w Ver. 05, Gaussian, Inc.).

2.3. Beckmann rearrangement of CHO

The rearrangement reaction for producing CPL from CHO was carried out as follows: 0.01 mol CHO and 0.02 mol DES were mixed and reacted at 80 °C for 2 h under nitrogen atmospheres. After the reaction is completed, the reactor was quickly cool to room temperature with a water bath. And the dichloromethane (2 times the volume of the reaction mixture) as the product CPL extractant was added into the reaction mixture to extract and separate of product for three times. Then the extracted phases was collected together and distilled to remove the extractant dichloromethane, obtaining the product CPL. The obtained product was quantified on an Agilent GC System 9000 equipped a DB-5 column (30 m × 0.25 mm × 0.25 μm). The conversion and selectivity were calculated by eqn (1) and (2) respectively; C_0 and C_1 stand for the initial content and remaining content of CHO respectively. C_2 stands for the content of CHO generated for CPL, in which the content was obtained by the area normalization method in GC. The CHO conversion and the CPL selectivity were calculated based on the following formulas:

$$\text{Conversion\%(CHO)} = \frac{C_0 - C_1}{C_0} \times 100\% \quad (1)$$

$$\text{Selectivity\%(CPL)} = \frac{C_2}{C_0 - C_1} \times 100\% \quad (2)$$

For the recovery of the DESs after the reaction, the residual dichloromethane in DES layer was removed by vacuum distillation, and the obtained DES was reused directly in the cycle of the experiment by the method described above. The experiments were repeated five times to determine the credibility of the obtained results.

3 Results and discussion

3.1. Characterization of the synthesized DESs

FT-IR spectra of $InCl_3$, AA, and the DES $[InCl_3][AA]_2$ were analyzed to confirm the structure and formation mechanism of the DES $[InCl_3][AA]_2$. As observed in Fig. 1a, a prominent absorption peak at 3200–3600 cm^{-1} is evident, which is ascribed to the hydrogen bonding interaction between Cl in $InCl_3$ and O–H in AA during the creation of hydrogen bonds in DES $[InCl_3][AA]_2$.[34] From the thermogravimetric curves in Fig. 1b, DES $[InCl_3][AA]_2$ begins to decompose about at 120 °C, and this decomposition temperature is obviously higher than the boiling point of acetic acid (AA), indicating that DES $[InCl_3]$

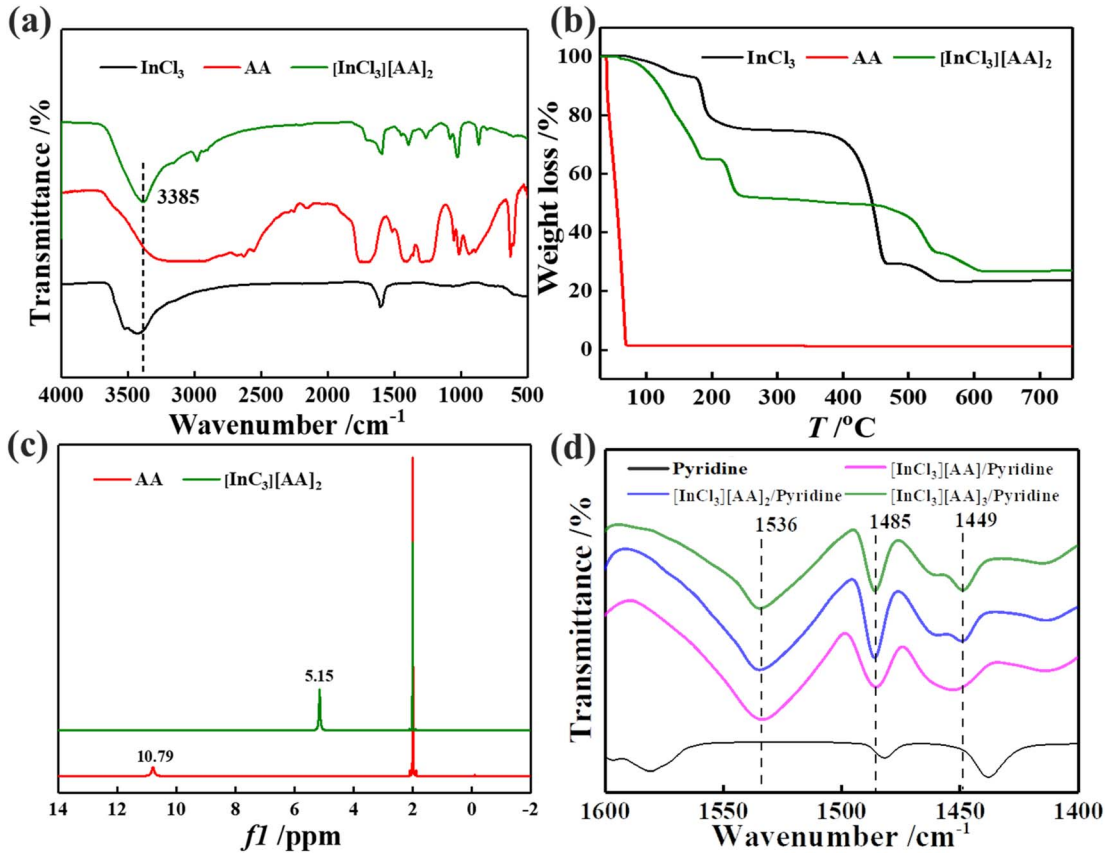

Fig. 1 (a) FT-IR spectra of $InCl_3$, AA and $[InCl_3][AA]_2$. (b) TG spectra of $InCl_3$, AA and $[InCl_3][AA]_2$. (c) ^1H NMR spectra of AA and $[InCl_3][AA]_2$ in DMSO. (d) FT-IR spectra were obtained using pyridine as the probe molecule, with a volume ratio of DES to pyridine being 1 : 2.

$[AA]_2$ has higher thermal stability than the reactant AA.[35] It was apparent that the strength of hydrogen bonds develops an significant role in the thermal stability of DES, and this hydrogen bonds in DES can effectively hinder the "escape" of AA molecules due to their high volatility at the high temperature, improving the retention of AA in the reaction system. It is worth noting that the changes in DES $[InCl_3][AA]_2$ after 120 °C exhibit a phenomenon of staged weight loss, indicating that the different components in DES decompose sequentially at different temperature. Samples AA and DES $[InCl_3][AA]_2$ were also characterized by ^1H NMR in deuterated dimethyl sulfoxide (d6-DMSO) to further determine the hydrogen bonding interactions in DES $[InCl_3][AA]_2$. As shown in Fig. 1c, comparing with ^1H NMR spectra of AA and DES $[InCl_3][AA]_2$, it is found that the active hydrogen on the hydroxyl group in acetic acid in DES $[InCl_3][AA]_2$ underwent a chemical shift, shifting from 10.79 ppm in acetic acid to 5.15 ppm, indicating an increase in the carboxylic acid hydroxyl hydrogen electronegativity of acetic acid, thus the hydrogen bonding forces between $InCl_3$ and AA forms.[36] As shown in Fig. 1d, the absorption vibrational peaks near 1536 cm^{-1} and 1449 cm^{-1} in the FT-IR spectrum of the pyridine probe are Brønsted and Lewis acidic sites, stem from the interact with pyridine to produce pyridine salt $[H\text{-pyridine}]^+$ and Lewis-pyridine complexes, respectively.[37] In addition, 1485 cm^{-1} is the absorption vibration peak generated by the synergistic effect of pyridine salt $[H\text{-pyridine}]^+$ and Lewis-pyridine complex. The aforementioned findings suggest that the synthesized DESs possess both Brønsted and Lewis dual acidity. Furthermore, as the AA content in the DESs increases, the intensity of the absorption peak at 1536 cm^{-1} rises, whereas the intensity of the absorption peak at 1449 cm^{-1} decreases with a reduction in $InCl_3$ content. This demonstrates that the acidity of the synthesized DESs can be effectively controlled, which is beneficial for selecting catalyst DESs with the appropriate acid strength for various reactions.

3.2. Theoretical study

To gain deeper insights into the formation mechanism of DESs, we employed DFT calculations and optimizations to determine their most stable configurations, as depicted in Fig. 2. Additionally, we utilized Multiwfn and Winvmd software to analyze the electrostatic potential (ESP) and reduced density gradient (RDG) of the DESs.[38–41] And DESs $[InCl_3][FA]_2$, $[InCl_3][AA]_2$, $[InCl_3][PA]_2$, $[InCl_3][BA]_2$, $[InCl_3][AA]$, $[InCl_3][AA]_3$ are investigated at the B3LYP/LanL2MB base group.[42,43]

3.2.1 Results of quantum structure analysis. The interaction between the Cl atom of $InCl_3$ and the H atom on the carboxyl group of Brønsted acids (such as FA, AA, PA, or BA) results in the formation of a new covalent bond (bond ①) with a bond length that falls within the hydrogen bond length range

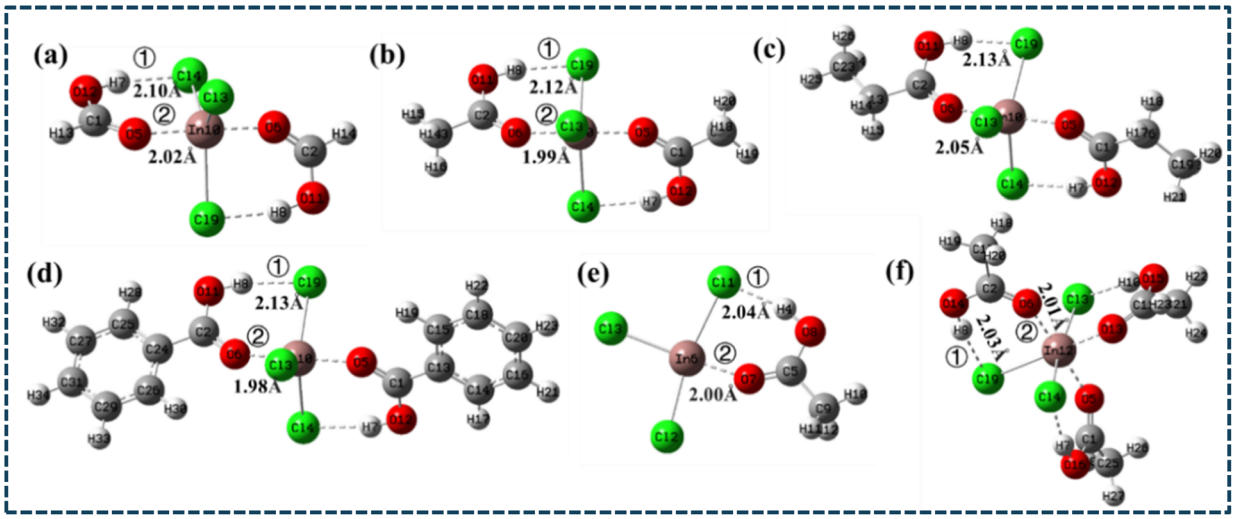

Fig. 2 Most stable structures of DESs: (a) $[InCl_3][FA]_2$, (b) $[InCl_3][AA]_2$, (c) $[InCl_3][PA]_2$, (d) $[InCl_3][BA]_2$, (e) $[InCl_3][AA]$, (f) $[InCl_3][AA]_3$.

of 2.0 to 2.2 Å, as illustrated in Fig. 2. This finding confirms the presence of hydrogen bond lattice interactions between $InCl_3$ and the organic acids, establishing that this bond is indeed a hydrogen bond interaction.[44] At the same time, the In atom of $InCl_3$ interacts with the O atom on the carbonyl group in organic acids to form a coordination bond (bond ②), further enhancing the stability of DESs attributed to the stable six membered ring.

3.2.2 Results of electrostatic potential (ESP) analysis. Fig. 3 shows electrostatic potential analysis diagram, the blue region characterises DES electronegative, and the darker it is, the stronger of its electronegativity. On the contrary, the red region represents DES electropositive, and the darker it is, the stronger of its electropositivity.[36] From the analysis results, it is seen that the H atom on the hydroxyl group of AA is electropositive, while the Cl atom in $InCl_3$ is electronegative, so both can interact with each other. At this time, the electronegative Cl atom in $InCl_3$ also interact with the electropositive region H in the organic acid molecules (FA, AA, PA, or BA), forming the hydrogen bonding. This result is in line with the results in Fig. 2, bond ①. More importantly, ESP results are in line with the structural optimization analysis in Fig. 2, further demonstrating the formation of hydrogen bonding.

3.2.3 Results of reduced density gradient (RDG) analysis. Fig. 4 represents the contrast figure of RDG with a blue-green-red scale with −0.04 to 0.02 au values of $\text{sign}(\lambda_2)\rho$. The notable atractions such as hydrogen bond and halogen bond is on the left with blue. The weak interaction such as van der Waals is in the middle shown with light green, while the steric repulsions are shown in red on the right. Fig. 5 presents the RDG contour maps, with Fig. 5b serving as an illustrative example to elucidate the formation process of the DES $[InCl_3][AA]_2$. A blue circular region is observed between the H atom on the carbonyl group of AA and the Cl atom in $InCl_3$, signifying the existence of a hydrogen bond between AA and $InCl_3$. Furthermore, the green

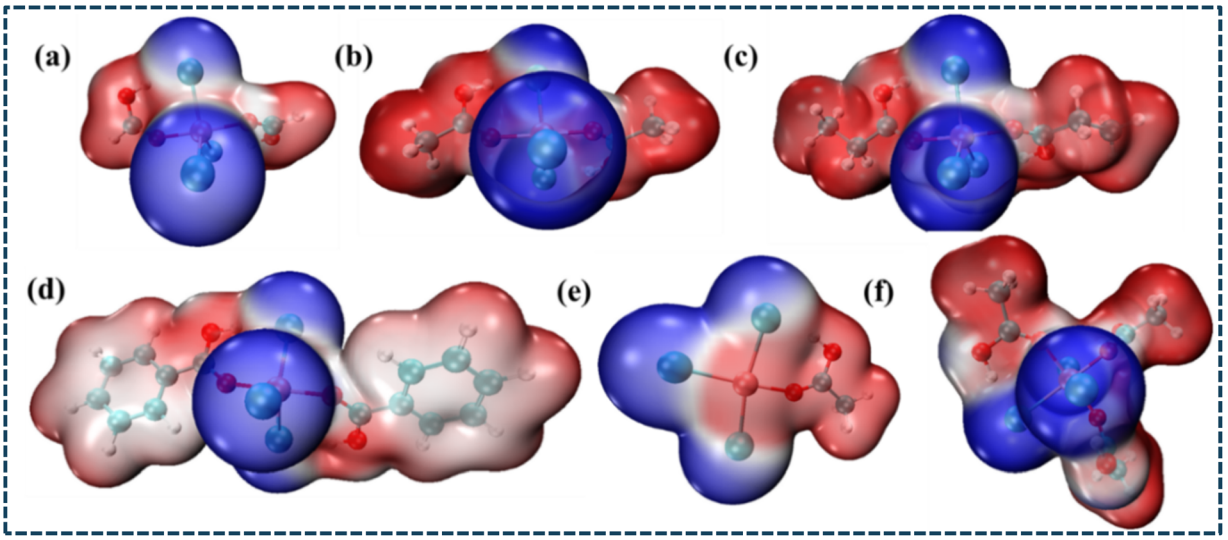

Fig. 3 DES ESP analysis: (a) $[InCl_3][FA]_2$, (b) $[InCl_3][AA]_2$, (c) $[InCl_3][PA]_2$, (d) $[InCl_3][BA]_2$, (e) $[InCl_3][AA]$, (f) $[InCl_3][AA]_3$.

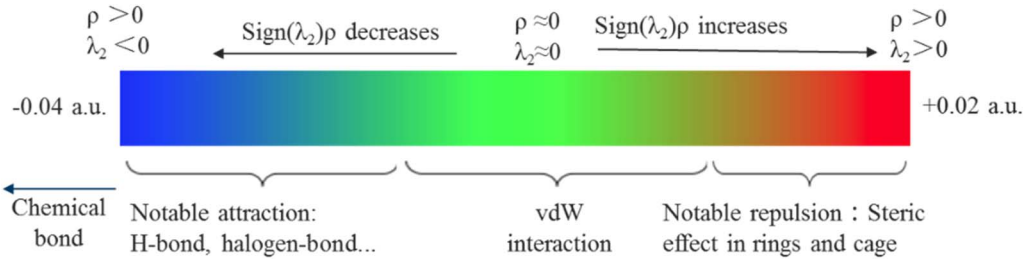

Fig. 4 Contrast caliper of RDG.

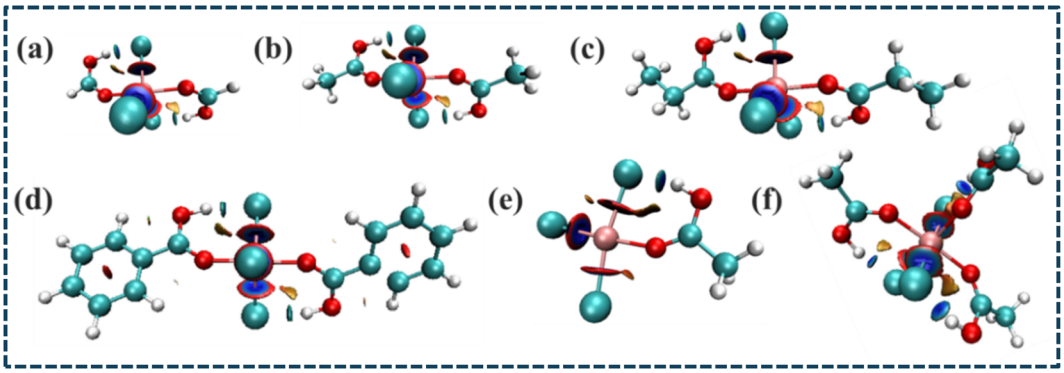

Fig. 5 DESs RDG analysis: (a) $[InCl_3][FA]_2$, (b) $[InCl_3][AA]_2$, (c) $[InCl_3][PA]_2$, (d) $[InCl_3][BA]_2$, (e) $[InCl_3][AA]$, (f) $[InCl_3][AA]_3$.

circular region between $InCl_3$ and AA suggests the presence of weak interaction forces, such as hydrogen bonding or van der Waals forces, between these two components. The interaction mode between $InCl_3$ and organic acids in other DESs $[InCl_3][FA]_2$, $[InCl_3][PA]_2$, $[InCl_3][BA]_2$, $[InCl_3][AA]$, $[InCl_3][AA]_3$ is basically similar to DES $[InCl_3][AA]_2$. Thus, the primary modes of interaction between $InCl_3$ and Brønsted acids are hydrogen bonding and van der Waals forces, aligning with the research findings that indicate DESs exhibit insufficient thermal stability (Fig. 1b), as non-covalent bonding between these types of organic compounds is easily broken at high temperature.

Usually, the strength of weak interactions of non-covalent bonds is closely related to the peaks in low density and low gradient areas. The more peaks in this region, the stronger the weak interaction.[45] Here, we take Fig. 6b as an example to explain the non-covalent bonds. There are more peaks in the low density area, indicating a hydrogen bonding effect between (AA) H⋯ Cl ($InCl_3$) in DES $[InCl_3][AA]_2$. Furthermore, the grid point density located at the bottom left of the electron cloud

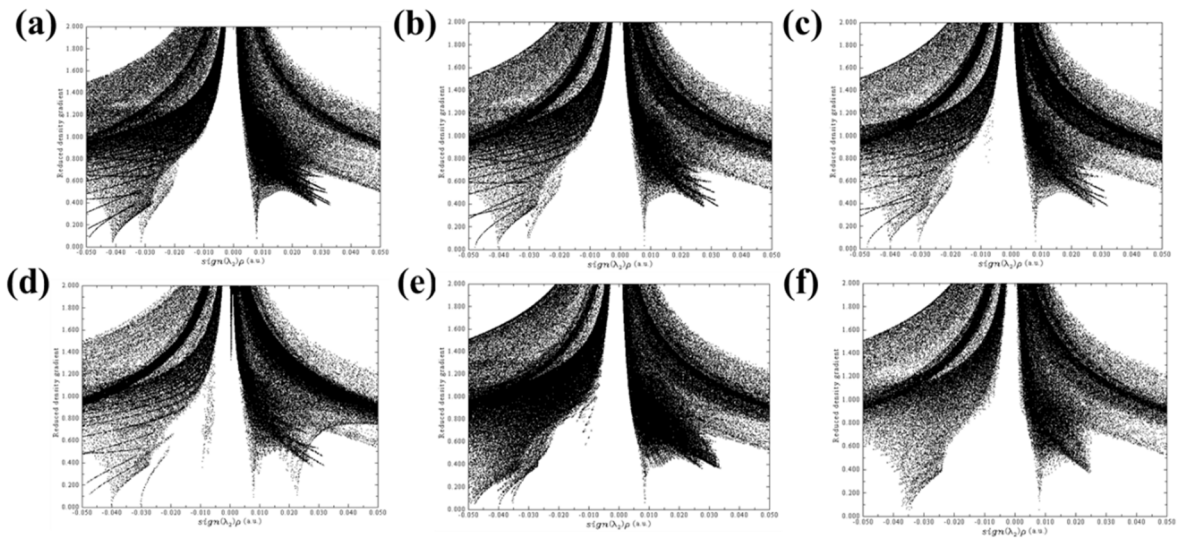

Fig. 6 RDG *vs.* sign(λ_2)ρ(au): (a) $[InCl_3][FA]_2$, (b) $[InCl_3][AA]_2$, (c) $[InCl_3][PA]_2$, (d) $[InCl_3][BA]_2$, (e) $[InCl_3][AA]$, (f) $[InCl_3][AA]_3$.

Table 2 Effects of different DESs on rearrangement reaction[a]

Entry	Samples	Acid strength[b]/mV	C_{CHO}/%	S/% CPL	S/% COX
1	$InCl_3$	802	35.4	60.7	16.5
2	AA	220	18.5	0	78.9
3	$[InCl_3][FA]_2$	630	100	32.4	67.6
4	$[InCl_3][AA]_2$	613	100	99.5	0.5
5	$[InCl_3][PA]_2$	591	89.7	90.2	9.8
6	$[InCl_3][BA]_2$	572	88.3	89.8	10.2
7	$[InCl_3][AA]$	566	84.6	85.8	14.2
8	$[InCl_3][AA]_3$	654	100	99.2	0.4

[a] DESs 0.02 mol (classified as a "compound" for the purpose of calculating its molecular weight) was used for the reaction, along with CHO (0.01 mol) at a temperature of 80 °C for 1.5 h. [b] A mixture of 2 mmol of DES and 30 mL of acetonitrile was prepared, and its initial potential was measured using a pH meter at 25 °C.

density map provides additional evidence of the weak interaction between van der Waals forces and hydrogen bonds. Therefore, DFT model explains the synergistic effect of establishing dynamic hydrogen bonds between components within the $InCl_3$-AA elastomer network in theory. Meanwhile, the hydrogen bonding interactions of DESs $[InCl_3][FA]_2$, $[InCl_3][PA]_2$ and $[InCl_3][BA]_2$ are strong, which is in line with the results in Fig. 3. Importantly, this characteristic provides favorable condition for the reaction and the catalyst recovery.

3.3. Effects of the types of DESs on the rearrangement reaction

Table 2 indicates that while $InCl_3$ possesses a relatively high acid strength (802 mV), its catalytic performance in catalyzing the rearrangement reaction is notably poor, as evidenced by entry 1. This may be because both $InCl_3$ and CHO are solid, and both cannot fully contact at the reaction temperature during the reaction process. Meanwhile, $InCl_3$ only has Lewis acidity and its acid strength is high, so the occurrence of side reaction is exacerbated. When AA is used as a catalyst, CHO conversion is only 18.5%, and the desired product CPL is not detected, indicating that low acid strength of catalyst cannot meet the requirement of the rearrangement reaction. Additionally, too low acid strength can result in side reactions (entry 2). Meanwhile, the synthesized diacid type DESs exhibit outstanding catalytic performance, with 84–100% CHO conversion and 85–99.2% CPL selectivity (entries 3–8), attributing to their diacid active sites and the synergistic catalytic effect between them. Furthermore, the acid strength plays a crucial role in influencing the reaction outcomes. As the acid strength of the DESs increases, the conversion rate of CHO shows an ascending trend. However, the selectivity towards CPL initially rises and then subsequently declines. Notably, among all the DESs investigated, DES $[InCl_3][AA]_2$ stands out with exceptional catalytic performance, achieving 100% CHO conversion and 99.5% CPL selectivity (entry 4). When DES $[InCl_3][AA]_3$ having high acid strength is used, CHO conversion is 100%, and CPL selectivity decreases by 0.3%, indicating that strong acid strength is detrimental to the reaction (entry 8). To conclude, the nature of the catalyst's acidity and an appropriate acid strength are pivotal in achieving high conversion rates and selectivity. Consequently, in the forthcoming experiments, DES $[InCl_3][AA]_2$ will serve as the catalyst to explore the impact of various other factors on the reaction.

3.4. Optimization of reaction conditions

The pivotal factors influencing the outcome of the reaction were examined, including the reaction temperature (T), reaction time (t), and the concentration of the DES $[InCl_3][AA]_2$ catalyst (Fig. 7). Notably, the role of temperature stands out as a crucial parameter in Fig. 7a. At a lower temperature of 60 °C, the CHO conversion rate is modest, achieving just 81.2%. However, elevating the temperature to 80 °C leads to a remarkable improvement, with CHO undergoing complete conversion and CPL selectivity soaring to 99.5%. This enhancement can be attributed to the endothermic nature of the CHO rearrangement reaction, where an increase in temperature facilitates the reaction's progress. Conversely, when the temperature surpasses 80 °C, a decline in CPL selectivity is observed, possibly stemming from undesirable side reactions that take place in the feedstock or the product under extreme thermal conditions.[46] Therefore, the suitable temperature for the rearrangement reaction is 80 °C. As depicted in Fig. 7b, a reaction period of 2 hours suffices to accomplish total CHO conversion, resulting in a CPL selectivity of 99.5%. This highlights the efficacy of the process in terms of rapid and selective conversion. Prolonging the reaction time reveals a downward trend in CPL selectivity, attributed to the heightened likelihood of side reactions emerging as the reaction progresses. Hence, an optimal reaction time of 2 h is established. Further analysis in Fig. 7c indicates that with 0.02 mol of DES, CHO conversion attains 100% efficiency. However, the CPL yield initially rises before declining with further DES addition.Excessive use of DES indicates that it accelerates the occurrence of side reactions and reduces the selectivity of CPL. In a word, the optimal reaction conditions are as below: n(CHO) : n(DES $[InCl_3][AA]_2$)1 : 2, reaction temperature 80 °C, and reaction time 2 h. Under the specified reaction conditions, CHO conversion achieves full efficiency at 100%, accompanied by a CPL selectivity of 99.5%.

The extraction method is used to separate reactant, target product, and by-products with the catalyst, and the separated DES $[InCl_3][AA]_2$ is recovered and reused in the rearrangement reaction to determine its reusability (Fig. 7d). Upon reuse for seven consecutive cycles, DES $[InCl_3][AA]_2$ retains substantial catalytic activity, with CPL selectivity remaining at a high level of 99%. This demonstrates the remarkable reusability of DES $[InCl_3][AA]_2$ in the reaction, likely attributed to the effective inhibition of catalytic active site depletion by hydrogen bonding interactions.

3.5. *E*-factor calculation and result analysis

In order to quantitatively evaluate the environmental efficiency of the current $[InCl_3]$[AA]-DES catalyzed Beckmann rearrangement reaction system, we calculated the *E*-factor

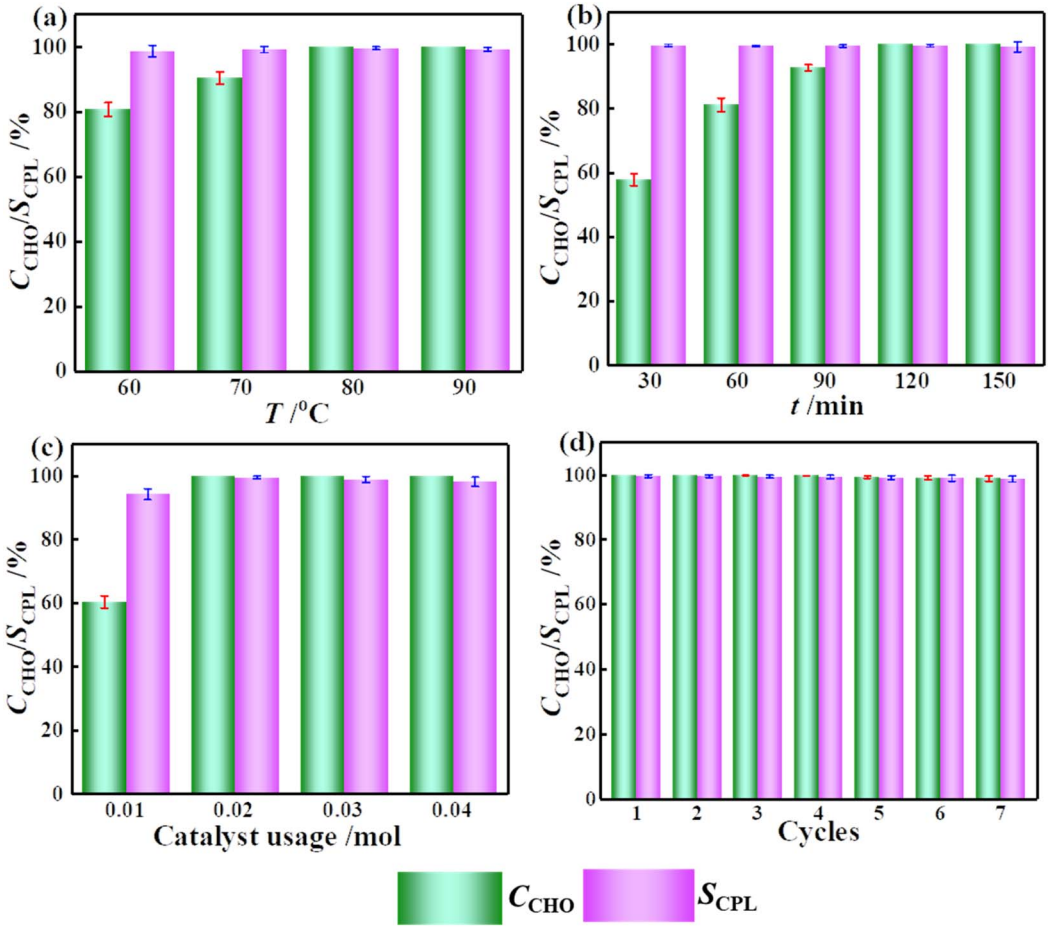

Fig. 7 Effects of reaction conditions on the performance and reusability of DES $[InCl_3][AA]_2$: (a) impact of reaction temperature. (b) effect of reaction time. (c) Influence of catalyst loading. (d) Assessment of DES reusability. The reaction was conducted using 0.02 mol of DES $[InCl_3][AA]_2$, 0.01 mol of CHO, at a temperature of 80 °C for 2 h. Error bars represent the standard deviation (SD).

(environmental factor). *E*-factor is an indicator for measuring the amount of waste generated in chemical processes, and its calculation formula is: *E*-factor = (total waste mass)/(target product mass).[47]

In our study, the total waste mass includes all non target products generated during the reaction process as well as all raw materials used in the reaction but ultimately not converted into the target product. By carefully analyzing the reaction process, we determined the types and quantities of these wastes and calculated the *E*-factor accordingly. The calculation results show that the *E*-factor value of the current $[InCl_3][AA]$-DES catalytic system is relatively low (approaching 0), indicating that the process performs well in waste generation and has high environmental efficiency. This result not only validates the potential of $[InCl_3][AA]$-DES as a green catalyst, but also further emphasizes its application prospects in the field of sustainable chemistry.

3.6. Reaction pathway and mechanism speculation over $[InCl_3][AA]_2$

The reaction product composition was examined using GC analysis, leading to the hypothesis of a rearrangement reaction pathway as illustrated in Fig. 8a. At the same time, the molecular structure of DES $[InCl_3][AA]_2$ is calculated and optimized using Gaussian 09 software at the B3LYP/LanL2MB group level. The optimization findings reveal that $InCl_3$ functions as a hydrogen bond acceptor, while AA serves as a hydrogen bond donor, fostering the formation of hydrogen bonds between the Cl atom in $InCl_3$ and the hydrogen atom of AA. The DFT outcomes indicate that none of the structures exhibit imaginary frequencies, suggesting a local minimum in each case.[42,43] Concurrently, the In atom demonstrates robust coordination capacity, enabling it to bind with the O atom of AA carbonyl group, constructing a stable six-membered ring structure that enhances the thermal stability of DES (Fig. 8b). This finding aligns with the observations from Fig. 1b. Drawing upon the experimental evidence, a plausible mechanism for the CHO rearrangement reaction catalyzed by DES $[InCl_3][AA]_2$ is proposed in Fig. 8c. Fig. 8c outlines the reaction sequence in seven distinct steps. Initially, the lone electron pairs on CHO's N atom coordinate with the In active center in DES $[InCl_3][AA]_2$, yielding the intermediate IC1 (step 1). Subsequently, the unoccupied coordination site of In in IC1 engages with the O atom of CHO, giving rise to the transition state TS1 (step 2), featuring an O–In–N ternary ring configuration. Next, the In–N bond

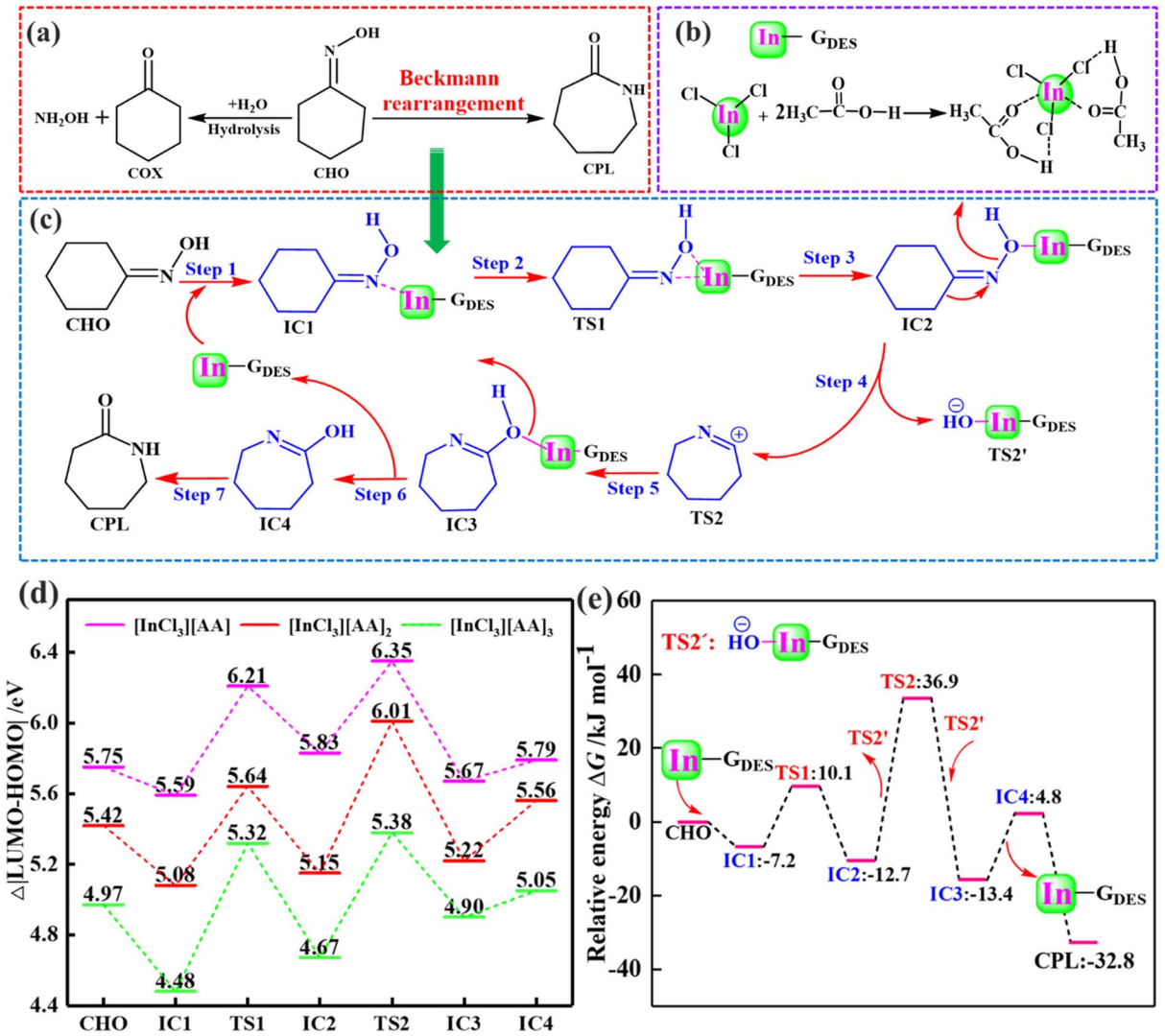

Fig. 8 (a) Rearrangement reaction path over $[InCl_3][AA]_2$. (b) DES $[InCl_3][AA]_2$ structure. (c) Mechanism speculation over $[InCl_3][AA]_2$. (d) Orbital energy gaps Δ|LUMO–HOMO| of CHO, transition states TS1–TS2 and intermediates IC1–IC4 over different DESs. (e) Relative free energy (Δ*G*) over $[InCl_3][AA]_2$.

dissociation results in the formation of intermediate IC2 (step 3). The electron density redistribution occurs within IC2, with the O atom's electron cloud shifting towards the electropositive In center, eliciting an inductive effect. This shift intensifies the N atom's electropositivity in IC2, encouraging CH_2 within CHO, now coordinated with hydroxyl groups, to present its covalent electron pairs (stemming from the CH_2–C bond's heterolytic cleavage) to attack the N atom in IC2. Simultaneously, the electron pair in the O–N covalent bond departs, leading to bond cleavage. As a result, two transition states are formed: TS2 with a seven-membered ring structure and TS2′ incorporating the catalytic active centers (step 4). This pivotal stage dominates the entire rearrangement process. Subsequently, an anion–cation pairing reaction between TS2 and TS2′ gives rise to intermediate IC3 (step 5). DES $[InCl_3][AA]_2$ detaches from IC3, yielding IC4 with an enol-like configuration (step 6), while DES $[InCl_3][AA]_2$ remains available to catalyze subsequent reactions. The concluding step involves the rearrangement of IC4's enol structure, ultimately producing the target product CPL (step 7).

3.7. Frontier molecular orbital analysis for reaction

The frontier molecular orbitals of the CHO rearrangement catalyzed by DES $[InCl_3][AA]_x$ ($x = 1$–3) are calculated using DFT. A comprehensive structural analysis and optimization were conducted for CHO, intermediates (IC1–IC4), transition states (TS1–TS2), and the product CPL. Additionally, the energy barriers, expressed as Δ|LUMO–HOMO|, were computed (Fig. 8d). Notably, all species in the reaction exhibit Δ|LUMO–HOMO| values below 6.3 eV, suggesting their effective activation by the DES catalysts.[41] Furthermore, a similar trend in Δ|LUMO–HOMO| variations is observed across all participating species. Δ|LUMO–HOMO| with the catalyst DES $[InCl_3][AA]_3$ has the lowest energy barrier, while DES $[InCl_3][AA]$ is used as the catalyst, the species Δ|LUMO–HOMO| is the highest. According to molecular orbital theory, Δ|LUMO–HOMO| serves as an

indicator of the electron's ability to transition from an occupied orbital to an unoccupied one, thereby providing insight into the reactivity of reactants within the reaction. Specifically, a lower Δ|LUMO–HOMO| value signifies an increased likelihood of electronic transitions occurring and, consequently, enhanced reactant activity.[48] Indeed, the lower Δ|LUMO–HOMO| values facilitate the conversion of CHO into the desired product CPL. Further confirmation comes from DFT calculations, which verify that each transition state (TS1–TS2′) possesses a single imaginary frequency and exhibits the highest energy at 0 K, confirming their structural reliability. Notably, the transition states (TS1–TS2) possess higher energy barriers compared to CHO and intermediates (IC1–IC4), emphasizing the significance of transition state stability in governing the reaction. Regarding the catalytic efficacy of various DESs for CHO conversion to CPL, their activity ranks from low to high as follows: DES $[InCl_3][AA]$ < DES $[InCl_3][AA]_2$ < DES $[InCl_3][AA]_3$, which is consistent with the acid strength results of the DESs catalytic reaction (Table 2).

3.8. Free energy for CHO conversion to CPL

As shown in Fig. 8e, the free energy of the reaction is calculated using DFT (ΔG) in DES $[InCl_3][AA]_2$ catalytic system. Specifically, the formation of intermediate IC1 from the reactant CHO is associated with an energy barrier of −7.2 kJ mol^{-1} (Fig. 8c step 1 and 8e), and then IC1 converts to the transition state TS1 (Fig. 8c step 2 and 8e) with an energy barrier of 17.3 kJ mol^{-1}. The energy barrier for the conversion of intermediate IC1 to IC2 is −5.5 kJ mol^{-1} (Fig. 8c step 3 and 8e), indicating that these three steps are easy to occur. The transition from intermediate IC2 to the transition states TS2 and TS2′ presents the highest energy barrier of 49.6 kJ mol^{-1} across the entire rearrangement process (Fig. 8c, step 4 and 8e). The intermediate IC3 arises from the anion–cation pairing ion reaction between transition states TS2 and TS2′, involving an energy barrier of −50.3 kJ mol^{-1} (Fig. 8c, step 5 and 8e). Subsequently, the DES is eliminated from IC3 to yield the enol intermediate IC4 (Fig. 8c step 6 and 8e), with an associated energy barrier of 18.2 kJ mol^{-1}. Finally, CPL formation from IC4 is a tautomerism of enol and ketone forms, with −32.8 kJ mol^{-1} (Fig. 8c, step 7 and 8e). In essence, the CHO conversion process within the DES $[InCl_3][AA]_2$ catalytic system exhibits a total free energy barrier of −32.8 kJ mol^{-1}, suggesting a facile reaction pathway. This observation aligns well with the low activation energy (E_a = 24.6 kJ mol^{-1}) derived from reaction kinetics analyses, further validating the efficiency of the catalytic system. The reason may be that in the catalytic system DES $[InCl_3][AA]_2$, the hydrogen bond connected to the Cl atom of $InCl_3$ improves the electropositivity of In, thereby enhancing its outstanding coordination ability. Moreover, the well-suited acidity of the B–L diacid DES $[InCl_3][AA]_2$, coupled with the synergistic catalysis of Brønsted and Lewis acids, collaboratively diminishes both the reaction energy barrier and the activation energy.

3.9. Reaction kinetics study

During the experiment, four reaction temperatures of 60 °C, 70 °C, 80 °C, and 90 °C are selected for kinetic analysis using a simple power law model/Arrhenius kinetics.[49] The impact of varying reaction temperatures on both CHO conversion and CPL yield is clearly depicted in Fig. 9a and b, respectively. With increasing of reaction temperature and prolonging of reaction time, CHO conversion continues to increase, and CPL yield shows a trend of first increase and then decrease. Under the condition of reaction at 80 °C for 2 h, CHO conversion is 100%, and CPL yield reaches 99.5% with prolonging the reaction time, CPL yield decreases. Concurrently, during the initial 30 minutes of the reaction, a linear correlation is observed between CHO conversion and CPL yield, both of which exhibit a direct proportionality to the reaction time at the chosen reaction temperatures.

The kinetics and linear regression results at different temperatures (Fig. S4†) are analyzed in DES $[InCl_3][AA]_2$. The findings indicate that the correlation coefficient exceeds 0.99, suggesting a direct proportionality between ln Y_{CPL} and reaction time across various temperatures. This implies that the process adheres to a first-order kinetic equation.[50–53] The conversion of CHO is directly related to the yield of CPL. The slopes of the straight lines are 0.1344 min^{-1}, 0.1570 min^{-1}, 0.1831 min^{-1}, and 0.2007 min^{-1}, representing the reaction rate constants (k) at temperatures of 60 °C, 70 °C, 80 °C, and 90 °C, respectively (Fig. S5†). From Fig. 9c, it can be concluded that E_a is 24.6 kJ mol^{-1}, which is lower than the reported in

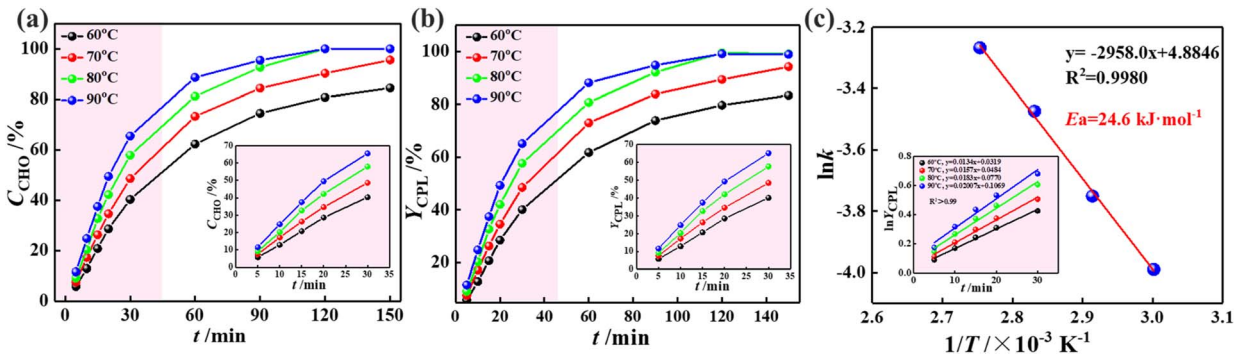

Fig. 9 (a) Effects of reaction temperature and time on CHO conversion. (b) Effects of reaction temperature and time on CPL yield. (c) Plot of ln k against 1/T. Reaction conditions: DES $[InCl_3][AA]_2$ 0.02 mol, CHO 0.01 mol.

literature.[46,50,54] This further confirms that DES $[InCl_3][AA]_2$ accelerates the reaction. The aforementioned outcomes align well with the computational results derived from DFT (Fig. 8e). CPL yield is 99.5% and the activation energy (E_a) of the reaction is 24.6 kJ mol^{-1} at 80 °C for 2 h. This indicates that DES has great potential for the preparation of CPL from CHO.

3.10. Universality

The rearrangement reaction of representative ketoximes is studied in the catalytic system DES $[InCl_3][AA]_2$ (Table 3). Primarily, aromatic ketone oximes, short-chain aliphatic ketone oximes, and cycloalkane ketone oximes that incorporate electron-donating and potent electron-withdrawing groups, including butanone oxime, acetone oxime, and cyclopentanone oxime, are chosen. It is observable that, within the DES $[InCl_3][AA]_2$ catalytic system, the conversion rate of aromatic ketoximes that possess strong electron-withdrawing substituents like $-NO_2$ is relatively low, achieving only 44.2% (entry 3). Conversely, aromatic ketoximes that bear electron-donating substituents such as $-CH_3$ can attain a complete conversion rate of 100% (entry 2), this may be attributed to the electronic effect of the reactant influencing its reactivity. The presence of an electron-donating group enhances the electron density of the lone electron pairs on the ketoxime's N atom, which in turn boosts its electronegativity. This results in a more effective interaction between the N atom and the In atom in the DES, leading to an increase in catalytic activity. In the case of short-chain aliphatic ketoximes and cycloalkane ketoximes, the conversion rates of the ketoximes lie between 90% and 98%

Table 3 Catalytic activity of DES $[InCl_3][AA]_2$ for various reactants[a]

Entry	Reactant	Conversion/%	Products	Selectivity/%
1	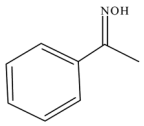	99.8	A: 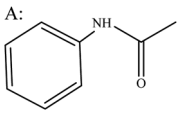	63.5
			B: 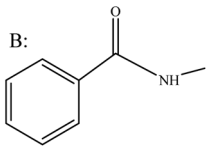	35.0
2	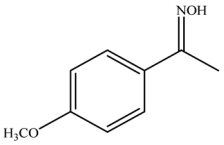	100	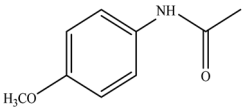	99.1
3	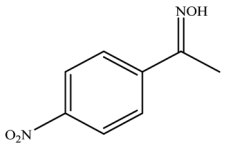	44.2	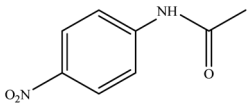	96.7
4		90.6	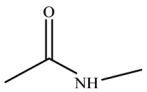	98.1
5	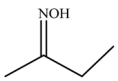	92.0	A: 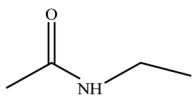	60.9
			B: 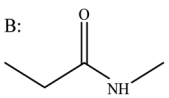	38.5
6	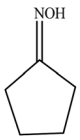	97.3	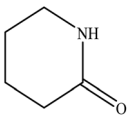	97.4

[a] Reaction conditions: DES $[InCl_3][AA]_2$ 0.02 mol, reactant 0.01 mol, $T = 80$ °C, $t = 2$ h.

(entries 4–6). Furthermore, we have observed that ketone oximes featuring asymmetric structures, like acetophenone oxime (entry 1) and butanone oxime (entry 5), produce two distinct products following the rearrangement reaction. Regarding the product distribution of acetophenone oxime, the selectivity towards products resulting from phenyl migration exceeds that of products arising from methyl migration. This may be owing to the migration power supply difference of migration group, and the group with strong power supply are more likely to migrate, resulting in higher product selectivity. The reactant butanone oxime also obtained similar results. From this, it can be seen that the stronger the electron donating performance, the easier it is to migrate, and the higher the selectivity of the resulting product. Overall, DES $[InCl_3][AA]_2$ demonstrates exceptional catalytic efficiency for the reaction involving various ketoximes. This remarkable performance can be attributed to the robust coordination and complexation capabilities of In within DES $[InCl_3][AA]_2$, as well as the synergistic effect between the two acidic active centers.

4 Conclusion

Task-specific DES with synergistic catalytic performance, using Lewis acid $InCl_3$ with multiple coordination numbers as the hydrogen bond acceptor and readily available organic acid as the hydrogen bond donor, are designed and synthesized for the catalytic reactions. The results show that the catalytic performance of DES $[InCl_3][AA]_2$ is outstanding. Under the optimal reaction conditions of DES $[InCl_3][AA]_2$ 0.02 mol, CHO 0.01 mol, reaction temperature 80 °C, and reaction time 2 h, reactant CHO conversion rate and target product CPL selectivity are 100% and 99.5%, respectively. In addition, DES $[InCl_3][AA]_2$ has outstanding reusability and universality. The DFT findings suggest that the combined catalytic effect stemming from hydrogen bonding forces, Brønsted and Lewis acidity sites, along with the high coordination number of the In atom, augments the capacity of the reaction's active center (In) to complex with transition states and intermediates. This, in turn, diminishes the reaction energy (E_a = 24.6 kJ mol^{-1} and ΔG = −32.8 kJ mol^{-1}) and promotes the progress of the reaction. This study has important academic significance and potential application prospects for the technological innovation of the clean production process of Beckmann rearrangement.

Data availability

The data supporting the findings of this study are available from the corresponding author upon reasonable request.

Conflicts of interest

There are no conflicts to declare.

Acknowledgements

This work was financially supported by the National Natural Science Foundation of China (22278232 and 22209090), the Weifang Science and Technology Plan Project (2022GX044), Shandong Provincial Natural Science Foundation Project (ZR2022QB098).

Notes and references

1 J. Eimontas, S. Yousef, N. Striūgas and M. Abdelnaby, *Renewable Energy*, 2021, **179**, 1385–1403.
2 X. Jin, R. Peng and W. Tong, *Catal. Today*, 2022, **405–406**, 193–202.
3 S. Liu, K. You, J. Song, R. Deng, F. Zhao, P. Liu, Q. Ai and H. a. Luo, *Appl. Catal., A*, 2018, **568**, 76–85.
4 S. Yin, B. Xu and Q. Zhu, *Chin. J. Catal.*, 2001, **22**, 494–496.
5 W. F. Hoelderich, R. Parton, F. Soulimani, F. Weckhuysen and B. J. Pccp, *Phys. Chem. Chem. Phys.*, 2016, **18**, 22636–22646.
6 A. Costa, P. M. Deyá, J. V. Sinisterra and J. Marinas, *Phys. Chem. Chem. Phys.*, 2011, **58**, 1266–1270.
7 Y. Y. Zhang, *Microporous Mesoporous Mater.*, 2018, **272**, 202–208.
8 K. Chaudhari, R. Bal, A. J. Chandwadkar and S. Sivasanker, *J. Mol. Catal. A:Chem.*, 2002, **177**, 247–253.
9 K. Wang, F. Wang and Y. Zhai, *Mol. Catal.*, 2023, **535**, 112881.
10 Z. W. Ge, *Catal. Lett.*, 2021, **151**, 1–11.
11 M. Hashimoto, Y. Obora and Y. Ishii, *Org. Process Res. Dev.*, 2009, **13**, 411–414.
12 C. Du, J. Zhang, L. Li, K. Wang and G. Luo, *AIChE J.*, 2019, **65**, e16603.
13 M. Ghiaci and M. Ghazaie, *Catal. Commun.*, 2016, **87**, 70–73.
14 Z. Wang, H. Ling, J. Shi, C. Stampfl, A. Yu, M. Hunger and J. Huang, *J. Catal.*, 2018, **358**, 71–79.
15 D. Li, D. Mao, J. Li, Y. Zhou and J. Wang, *Appl. Catal., A*, 2016, **510**, 125–133.
16 K. Elango, R. Srirambalaji and G. Anantharaman, *Tetrahedron Lett.*, 2007, **48**, 9059–9062.
17 D. Mao, Z. Long, J. Li and X. Wang, *RSC Adv.*, 2014, **4**, 15635.
18 S. Guo, Z. Du, S. Zhang, D. Li, Z. Li and Y. Deng, *Green Chem.*, 2006, **8**, 296–300.
19 S. Kurt, J. Horny, R. Horn, S. Koch and D. Moosburger-Will, *J. Appl. Polym. Sci.*, 2021, **138**, 29a30.
20 L. Lu, B. Zhang, H. Li, Y. Chao, Y. Li, L. Chen, H. Li, H. Ji, P. Wu and W. Zhu, *Mol. Catal.*, 2021, **512**, 111757.
21 E. Unlu, A. Arikaya and S. Taka, *Green Process. Synth.*, 2019, **8**, 355–372.
22 S. E. Hooshmand, S. Kumar, I. Bahadur, T. Singh and R. S. Varma, *J. Mol. Liq.*, 2023, **371**, 121013.
23 K. Pang, Y. Hou, W. Wu, W. Guo, W. Peng and K. Marsh, *Green Chem.*, 2012, **14**, 2398–2401.
24 H. Cruz, N. Jordao, A. L. Pinto, M. Dionisio, L. A. Neves and L. C. Branco, *ACS Sustain. Chem. Eng.*, 2020, **8**, 10653–10663.
25 E. A. Drylie, D. S. Wragg, E. R. Parnham, P. S. Wheatley, A. M. Z. Slawin, J. E. Warren and R. E. Morris, *Angew. Chem., Int. Ed.*, 2007, **46**, 7839–7843.
26 Q. Wang, X. Yao, Y. Geng, Q. Zhou, X. Lu and S. Zhang, *Green Chem.*, 2015, **17**, 2473–2479.
27 S. Long, Y. Feng, B. Chen, L. Gan, X. Zeng, M. Long and J. Liu, *Mol. Catal.*, 2023, **541**, 113106.

28 S. E. Hooshmand, S. Kumar, I. Bahadur, T. Singh and R. S. Varma, *J. Mol. Liq.*, 2023, **371**, 121013.
29 S. Sun, S. Liu, F. Yu, J. Zhang, W. Xing and S. Yu, *ACS Sustain. Chem. Eng.*, 2022, **10**(4), 1675–1688.
30 S. Sun, S. Liu, F. Yu, J. Zhang, W. Xing and S. Yu, *Chem. Eng. Sci.*, 2022, **253**, 117519.
31 J. Wang, X. Jiang, A. Shi, H. Yu, Q. Wu, Z. Liu, Z. Wang, S. Yu and S. Liu, *ACS Sustain. Chem. Eng.*, 2024, **12**, 1095–1103.
32 S. Sun, Y. Li, R. Sun, L. Jiao, S. Liu and S. Yu, *Fuel*, 2024, **357**, 129777.
33 T. Hou, B. Yu, M. Tao, L. Chen and Z. Qi, *ChemCatChem*, 2024, e202401563.
34 Y. Jiang, W. Zhu, H. Li, S. Yin, H. Liu and Q. Xie, *ChemSusChem*, 2011, **4**, 399–403.
35 L.-X. Dai, K. Koyama, M. Miyamoto and T. Tatsumi, *Appl. Catal., A*, 1999, **189**, 237–242.
36 A. D. Marinkovic, B. Z. Jovanovic, N. Todorovic and I. Juranic, *J. Mol. Struct.*, 2009, 920.
37 M. G. Mazzotta, D. Gupta, B. Saha, A. K. Patra, A. Bhaumik and M. M. Abu-Omar, *ChemSusChem*, 2014, **7**, 2342–2350.
38 D. Abranches, L. Silva, M. Martins, S. Pinho and J. Coutinho, *ChemSusChem*, 2020, **13**, 18.
39 M. Shakourian-Fard, S. M. Taimoory, H. R. Ghenaatian, G. Kamath and J. F. Trant, *J. Mol. Liq.*, 2021, **327**, 114850.
40 Y. Fu, M. Zhang, H. Qu, K. Liu, Z. Zhang, Y. Yang, B. Li, F. Liu and L. Wang, *J. Mol. Struct.*, 2020, **1206**, 127697.
41 T. Lu and Q. Chen, *J. Mol. Model.*, 2020, **11**, 26.
42 A. Gutiérrez, M. Atilhan and S. Aparicio, *J. Phys. Chem. B*, 2020, **124**, 1794–1805.
43 X. Zhao, G. Zhu, L. Jiao, F. Yu and C. Xie, *Chem.–Eur. J.*, 2018, **24**, 11021–11032.
44 S. L. Perkins, P. Painter and C. M. Colina, *J. Phys. Chem. B*, 2013, **117**, 10250–10260.
45 L. Ding, X. Sun, C. Huang, J. Li and B. Chen, *Mol. Catal.*, 2023, **538**, 113008.
46 J. S. Zhang, A. Riaud, K. Wang, Y. C. Lu and G. S. Luo, *Catal. Lett.*, 2014, **144**, 151–157.
47 X. Zhang, *Tactical Missile Technol.*, 2012.
48 X. Ye, M. Qi, H. Yang, F. S. Mediko, H. Qiang, Y. Yang and C. He, *Chem. Eng. Sci.*, 2022, **247**, 117017.
49 C. Ge, Z. Li, G. Chen, Z. Qin, X. Li, T. Dou, M. Dong, J. Chen, J. Wang and W. Fan, *Chem. Eng. Sci.*, 2016, **153**, 246–254.
50 C. Du, J. Zhang and G. Luo, *AIChE J.*, 2018, **64**, 571–577.
51 N. T. Zuidhof, M. H. J. M. de Croon, J. C. Schouten and J. T. Tinge, *Chem. Eng. Technol.*, 2013, **36**, 1387–1394.
52 N. T. Zuidhof, M. H. J. M. de Croon, J. C. Schouten and J. T. Tinge, *Chem. Eng. Technol.*, 2012, **35**, 1257–1261.
53 J. Zhang, C. Dong, C. Du and G. Luo, *Org. Process Res. Dev.*, 2015, **19**, 352–356.
54 L. Ronchin, A. Vavasori and M. Bortoluzzi, *Catal. Commun.*, 2008, **10**, 251–256.